Smart Structures and Systems, *Vol. 33*, *No. 1* (*2024*) *27-39*
https://doi.org/10.12989/sss.2024.33.1.027

Serviceability-oriented analytical design of isolated liquid damper for the wind-induced vibration control of high-rise buildings

Zhipeng Zhao [2a], Xiuyan Hu[*1], Cong Liao [2], Na Hong [3] and Yuanchen Tang [2]

[1] *School of Urban Construction and Safety Engineering*, *Shanghai Institute of Technology*, *Shanghai 201418*, *China*
[2] *Department of Disaster Mitigation for Structures*, *Tongji University*, *Shanghai 200092*, *China*
[3] *Institute of Earthquake Protection and Disaster Mitigation*, *Lanzhou University of Technology*, *Lanzhou 730050*, *China*

(*Received June 28*, *2022*, *Revised December 5*, *2023*, *Accepted December 11*, *2023*)

Abstract. The effectiveness of conventional tuned liquid dampers (TLDs) in controlling the wind-induced response of tall flexible structures has been indicated. However, the impaired control effect in the detuning condition or a considerably high mass cost of liquid may be incurred in ensuring the high-level serviceability. To provide an efficient TLD-based solution for wind-induced vibration control, this study proposes a serviceability-oriented optimal design method for isolated TLDs (ILDs) and derives analytical design formulae. The ILD is implemented by mounting the TLD on the linear isolators. Stochastic response analysis is performed for the ILD-equipped structure subjected to stochastic wind and white noise, and the results are considered to derive the closed-form responses. Correspondingly, an extensive parametric analysis is conducted to clarify a serviceability-oriented optimal design framework by incorporating the comfort demand. The obtained results show that the high-level serviceability demand can be satisfied by the ILD based on the proposed optimal design framework. Analytical design formulae can be preliminarily adopted to ensure the target serviceability demand while enhancing the structural displacement performance to increase the safety level. Compared with conventional TLD systems, the ILD exhibits higher effectiveness and a larger frequency bandwidth for wind-induced vibration control at a small mass ratio.

Keywords: analytical design; isolation; serviceability; tuned liquid damper; wind loads

1. Introduction

Wind loads are dominant environmental excitations for civil structures, which may produce critical damage or serviceability problems for structures (Soong and Spencer 2002, Kareem 2020). In such cases, serviceability-based design for engineering structures has attracted increasing attention as a promising solution to ensure satisfactory floor accelerations below predetermined thresholds (Huang *et al*. 2012, Chen *et al*. 2019, Gaur *et al*. 2020). As an effective solution to enhance user comfort, structural control devices, especially dynamic vibration absorbers (Lu *et al*. 2016, Elias and Matsagar 2017, Marian and Giaralis 2017, Niu *et al*. 2018, Roy *et al*. 2019), have been widely accepted to mitigate the wind-induced responses of dynamically excited structures according to the comfort requirement. Various dynamic vibration absorbers (Elias and Matsagar 2017, 2018, Yucel *et al*. 2019, Zhao *et al*. 2020, Wang *et al*. 2021, Islam and Jangid 2022) have been developed for a series of engineering projects, among which, tuned liquid dampers (TLDs) (Yalla and Kareem 2000, Tanveer *et al*. 2020) are widely adopted owing to the advantages of easy manufacturing, simple installation, functional versatility, and low maintenance cost. Combining wind-induced vibration control and daily functionalities of water storage or firefighting, several high-rise buildings have been equipped with TLDs (Tamura *et al*. 1995, Banerji *et al*. 2000, Suthar and Jangid 2021a, b, 2022). By exploiting liquid inertia, Sato (1987) proposed the concept of TLDs for dynamic absorption and vibration suppression. Inspired by this simple mechanical layout, liquid-related variants were developed, including tuned liquid column dampers (Mensah and Duenas-Osorio 2014), hybrid tuned liquid mass dampers (Love *et al*. 2019, Lee *et al*. 2021), inerter-based tuned liquid dampers (Zhao *et al*. 2019, Wang *et al*. 2021), and semi-active or active TLDs (Yalla *et al*. 2001). To realize the analytical design for wind-induced vibration control, Chang and Qu (1998) derived unified design formulae to determine the optimal properties of four TLD-based dampers. The existing research on wind-excited structures demonstrated that TLDs can effectively suppress structural acceleration, especially on the top floor, although a high weight penalty is unavoidable. To adequately utilize the potential of TLDs for wind-induced vibration control, the optimal tuning frequency and damping effect must be achieved. However, because the liquid damping is always less than the optimal value (Tait 2008), the liquid sloshing frequency may be indeterminate due to daily usage, leading to inadequate control of the peak response and a narrow frequency bandwidth for effective control.

To alleviate these disadvantages, certain modification methods involving screens (Tait *et al*. 2008, Love and Tait

*Corresponding author, Ph.D., Lecturer,
E-mail: hxy@sit.edu.cn
[a] Ph.D., Assistant Professor,
E-mail: zhaozhipeng@tongji.edu.cn

ISSN: 1738-1584 (Print), 1738-1991 (Online)

2010) to mobilize the liquid damping effect were introduced. Notably, the additional obstacles in the liquid tank hindered the expected functionality and likely incurred higher installation and maintenance costs. As an effective solution implemented outside the liquid tank, a compliant tuned liquid column damper (Pandey *et al*. 2019) was established by combining the liquid element with elastomeric pads and springs. Considering a linear isolation subsystem consisting of a linear spring and dashpot in parallel (Jangid and Datta 1995, Jangid and Banerji 1998), this study focuses on isolated liquid dampers (ILDs) because of their easy implementation and clear physical meaning. ILDs may provide an effective method to use the existing liquid tanks in buildings as a vibration control device for wind loads without hindering the original functionality of a liquid tank. The existing research on ILDs mainly focused on the effectiveness of seismic response control and isolation-based experiments (Furtmüller *et al*. 2019). However, despite the observed effect on the vibration control of wide frequency-band excitation, easy-to-understand analytical design formulae remain to be established, which limit the practical applicability and preliminary design of such devices. Furthermore, it is necessary to consider the inherent differences associated with the narrow frequency band, for instance, in terms of the wind loads, potential benefit, vibration control mechanism, and design method, which considerably influence the serviceability upgrading of wind-excited structures., which considerably influence the serviceability upgrading of wind-excited structures.

Considering this aspect, this study proposes a serviceability-oriented optimal design methodology for ILDs and derives analytical design formulae for practical use. The configuration and theoretical analysis model of the ILD are established, which are used to perform a stochastic response analysis to obtain the closed-form responses of the ILD-equipped structure subjected to stochastic wind and white noise. Correspondingly, an extensive parametric analysis is conducted, which yields a serviceability-oriented optimal design framework for the ILD incorporating the structural comfort demand. The ILD is applied to a typical high-rise building subjected to experimental wind loads to illustrate the effectiveness of the devices and proposed design method.

2. Dynamics of isolated liquid damper (ILD)

2.1 ILD configuration

The proposed ILD (Fig. 1) is composed of a tuned liquid subsystem and an isolation subsystem at the bottom. Assuming that the liquid sloshing response is lower than the fluid depth, the potential flow model is adopted in this study for its concise expression and accuracy for the deep liquid tank (Sun and Fujino 1994, Tait *et al*. 2008). The liquid movement can be simulated by the oscillations of the convective mass m_c and the impulsive mass m_i (Hu *et al*. 2023a), while the isolation subsystem can be treated as a horizontal spring with stiffness k_i and a dashpot with damping coefficient c_i in parallel (Lu *et al*. 2020a, b, Zhao

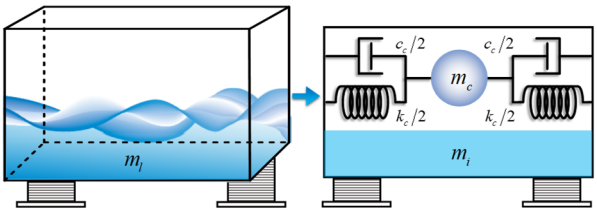

Fig. 1 Diagram of the isolated liquid damper (ILD)

et al. 2021, 2022, 2023, Hu *et al*. 2023b). Specifically, the isolating stiffness can be easily realized by typical elastomeric bearings or nature rubber bearings, while the desired damping property can be realized by the linear viscous damper. On the contrary to the conventional TLD, by connecting the liquid subsystem to the controlled structure through the isolation subsystem, the impulsive mass m_i oscillates in sync with the liquid tank wall (or isolation layer), while the convective mass m_c experiences sloshing motions. With regard to a rigid rectangular liquid tank (Fig. 1) with length L and width b, the liquid inside has depth h and density ρ, and the liquid mass is $m_l = \rho bhL$. For calculation efficiency, the simulation of the sloshing response is built through the potential flow model (Ruiz *et al*. 2016). Then, the expressions of the fundamental natural frequency of liquid sloshing ω_c, convective mass m_c, and impulsive mass m_i can be derived as (Bauer 1984)

$$\begin{cases} \omega_c = \sqrt{\dfrac{\pi g}{L}\tanh\left(\dfrac{\pi h}{L}\right)} \\ m_i = m_l - m_c \\ m_c = \beta m_l = \dfrac{8L}{\pi^3 h}\tanh\left(\dfrac{\pi h}{L}\right) m_l \end{cases} \tag{1}$$

where g and β, respectively, signify the gravitational acceleration and convective mass ratio. The liquid sloshing movement can be represented by the oscillation of a convective mass m_c, which is connected to the liquid tank by a linear convective spring with stiffness $k_c = m_c\omega_c^2$ and a dashpot with damping coefficient $c_c = 2\xi_c m_c\omega_c$ in parallel. ξ_c represents the inherent damping ratio of the liquid.

2.2 Governing equation of the ILD-equipped structure

To clarify the vibration control benefit of the ILD in Fig. 2, a linear damped single degree of freedom (SDOF) structure with a structural mass m, linear spring k, and viscous damping coefficient c is considered to quantify the dynamic responses of the ILD-equipped structure. Considering the external force excitation f, the governing motion equation can be expressed in the matrix form as

$$\boldsymbol{M}\ddot{\boldsymbol{u}} + \boldsymbol{C}\dot{\boldsymbol{u}} + \boldsymbol{K}\boldsymbol{u} = \boldsymbol{f} \tag{2}$$

The mass matrix $\boldsymbol{M}$, damping matrix $\boldsymbol{C}$, and stiffness matrix $\boldsymbol{K}$ of the SDOF structure controlled by a single ILD and the structural response vector $\boldsymbol{u}$ and external excitations vector $\boldsymbol{f}$ can be expressed as

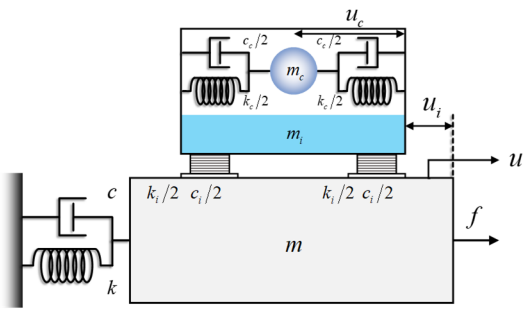

Fig. 2 Mechanical model of an SDOF structure with an ILD

$$\boldsymbol{M}=\begin{bmatrix} m+m_i+m_c & m_i+m_c & m_c \\ m_i+m_c & m_i+m_c & m_c \\ m_c & m_c & m_c \end{bmatrix},$$
$$\boldsymbol{C}=\begin{bmatrix} c & & \\ & c_i & \\ & & c_c \end{bmatrix}, \boldsymbol{K}=\begin{bmatrix} k & & \\ & k_i & \\ & & k_c \end{bmatrix}, \quad (3)$$
$$\boldsymbol{f}=\begin{Bmatrix} f \\ 0 \\ 0 \end{Bmatrix}, \boldsymbol{u}=\begin{Bmatrix} u \\ u_i \\ u_c \end{Bmatrix}$$

where u, u_i, and u_c denote the displacements of the primary structure, isolation layer deformation in the ILD, and displacement of the convective mass relative to the liquid storage tank, respectively.

2.3 Verification of the mechanical model of SDOF structure with ILD

The simplified mechanical model of the ILD-equipped SDOF structure in Section 2.2 is further verified in this section by using the coupled Euler-Lagrange (CEL) method, albeit the potential flow model itself is highly accurate for the simulation of liquid sloshing in a container. Considering an SDOF structure with the natural circular frequency of 2π rad/s, the mass and stiffness are, respectively, 20 tons and 790 kN/m. For the parameters of ILD, the stiffness of the isolator is ^{14} kN/m and the damping coefficient is $0.25\,\mathrm{kN\cdot s/m}$, while the dimensions of the liquid element are $L \times h \times b = 2.0\,\mathrm{m} \times 1.2\,\mathrm{m} \times 0.16\,\mathrm{m}$. The finite element software ABAQUS is adopted to establish the isolator and the primary structure along with the CEL model of the liquid element as shown in Fig. 3(a). The Eulerian liquid element is stationary and required to be able to contain the entire region of liquid movement. And the connector elements are adopted for the simulation of the isolator and the structure. The explicit dynamic analysis is performed under sinusoidal excitation, of which the liquid sloshing movement is shown Fig. 3(b). The dynamic responses including the base shear force and the displacement of the primary structure are recorded and compared to those obtained by ETABS using the simplified model. Upon analyzing and comparing response results

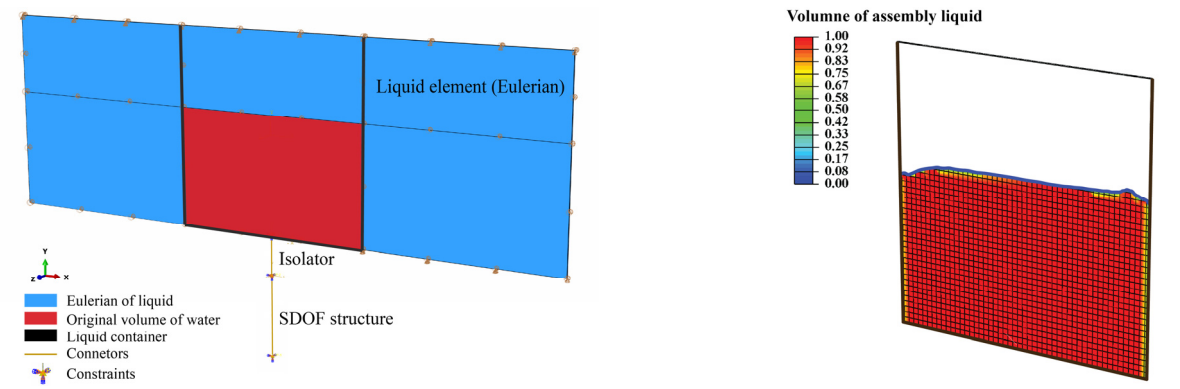

(a) (b)

Fig. 3 Schematic model of the ILD-equipped SDOF structure simulated by the CEL method: (a) finite element model and (b) the liquid sloshing movement in the finite element analysis model under dynamic excitation (the color legend indicates the volume of liquid in each mesh grid)

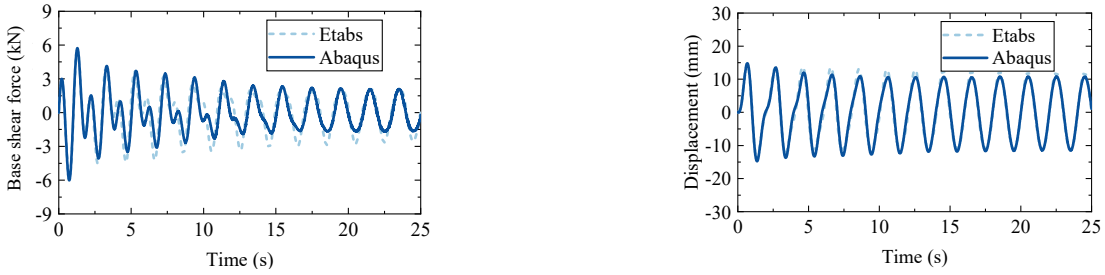

(a) (b)

Fig. 4 Dynamic responses of the ILD-equipped SDOF structure through the CEL method: (a) base shear force; and (b) displacement of the primary structure

Fig. 4, it becomes evident that the introduction of isolation bearings effectively mitigates the sloshing motion of the liquid. Consequently, ETABS achieves a relatively precise linear simulation of sloshing motion compared to the results obtained in ABAQUS.

2.4 Stochastic response analysis and analytical solution

To facilitate the dimensionless analysis, the key parameters of the ILD can be defined as the isolation frequency ratio κ, isolation damping ratio ξ, liquid mass ratio μ, and liquid sloshing ratio η, as indicated in Table 1. The structural parameters include the circular frequency ω and inherent damping ratio ζ. Substituting the dimensionless parameters listed in Table 1 into Eq. (3), the system matrices can be re-expressed as

$$\begin{cases} \widetilde{\boldsymbol{M}} = \begin{bmatrix} 1+\mu & \mu & \mu\beta \\ \mu & \mu & \mu\beta \\ \mu\beta & \mu\beta & \mu\beta \end{bmatrix}, \\ \widetilde{\boldsymbol{C}} = \begin{bmatrix} 2\zeta\omega_s & & \\ & 2\mu\xi\omega_s & \\ & & 2\mu\beta\xi_c\eta\omega_s \end{bmatrix} \\ \widetilde{\boldsymbol{K}} = \begin{bmatrix} \omega_s^2 & & \\ & \mu\kappa^2\omega_s^2 & \\ & & \mu\beta\eta^2\omega_s^2 \end{bmatrix}, \tilde{\boldsymbol{f}} = \begin{Bmatrix} \bar{f} \\ 0 \\ 0 \end{Bmatrix}, \boldsymbol{u} = \begin{Bmatrix} u \\ u_i \\ u_c \end{Bmatrix} \end{cases} \tag{4}$$

where superscript "~" denotes the dimensionless form of the matrices, and $\bar{f}$ refers to the external force-induced excitation imposed on the primary structure.

Expressing the equilibrium relationship in the Laplace domain, Eqs. (2)-(4) can be rewritten as

$$s^2\widetilde{\boldsymbol{M}}\boldsymbol{U} + s\widetilde{\boldsymbol{C}}\boldsymbol{U} + \widetilde{\boldsymbol{K}}\boldsymbol{U} = \widetilde{\boldsymbol{F}}, \tag{5}$$

where $s = i\Omega$, and $\boldsymbol{U}$ is the Laplace transform of the displacement vector $\boldsymbol{u}$ including U, U_i, and U_c. $\widetilde{\boldsymbol{F}} = \{F \quad 0 \quad 0\}^T$ is the Laplace transform of $\tilde{\boldsymbol{f}}$. Ω is the circular frequency of external excitation. To address the algebraic analysis problem expressed in Eq. (5), the external force-induced responses can be easily determined as

Table 1 Parameters for an SDOF structure with an ILD

Parameters	Definition	Description
Primary structure	ω_s	Circular frequency
	$\zeta = \dfrac{c}{2\omega_s m}$	Inherent damping ratio
ILD	ω_c	Liquid frequency
	ξ_c	Liquid damping ratio
	β	Convective mass ratio
	$\kappa = \dfrac{\sqrt{\frac{k_i}{m_l}}}{\omega_s}$	Isolation frequency ratio
	$\xi = \dfrac{c_i}{2\sqrt{m_l k_i}}$	Isolation damping ratio
	$\mu = \dfrac{m_l}{m}$	Liquid mass ratio
	$\eta = \dfrac{\omega_c}{\omega_s}$	Liquid frequency ratio

Correspondingly, structural displacement and acceleration transfer functions can be obtained as

$$H_U(s) = \frac{U(s)}{F(s)}, \qquad H_A(s) = \frac{s^2U(s)}{F(s)}. \tag{7}$$

Considering an external excitation with a spectral amplitude S_f, the mean square of the displacements σ_U^2 and accelerations σ_A^2 of the SDOF-ILD system can be obtained as (Crandall and Mark 1963)

$$\sigma_U^2 = \int_{-\infty}^{\infty} |H_U(s)|^2 S_f ds, \sigma_A^2 = \int_{-\infty}^{\infty} |H_A(s)|^2 S_f ds. \tag{8}$$

Adopting white noise with a constant spectral amplitude S_0 as a reference, the mean-square responses pertaining to the structural displacement can be derived in the closed form as

$$\begin{cases} U(s) = \dfrac{F(s)(s^4(-1+\beta) - 2s^3\xi\omega_s - s^2(\eta^2+\kappa^2)\omega_s^2 - 2s\eta^2\xi\omega_s^3 - \eta^2\kappa^2\omega_s^4)}{\begin{pmatrix} s^6(-1+\beta) + 2s^5(-1+(-1+\beta)\mu)\xi\omega_s + s^4(-1+\beta-\eta^2-\kappa^2-\kappa^2\mu+\beta\kappa^2\mu)\omega_s^2 \\ -2s^3\big(1+\eta^2(1+\mu)\big)\xi\omega_s^3 - s^2\left(\kappa^2+\eta^2\big(1+\kappa^2(1+\mu)\big)\right)\omega_s^4 - 2s\eta^2\xi\omega_s^5 - \eta^2\kappa^2\omega_s^6 \end{pmatrix}}, \\ U_i(s) = \dfrac{F(s)s^2(-s^2(-1+\beta) + \eta^2\omega_s^2)}{\begin{pmatrix} s^6(-1+\beta) + 2s^5(-1+(-1+\beta)\mu)\xi\omega_s + s^4(-1+\beta-\eta^2-\kappa^2-\kappa^2\mu+\beta\kappa^2\mu)\omega_s^2 \\ -2s^3\big(1+\eta^2(1+\mu)\big)\xi\omega_s^3 - s^2\left(\kappa^2+\eta^2\big(1+\kappa^2(1+\mu)\big)\right)\omega_s^4 - 2s\eta^2\xi\omega_s^5 - \eta^2\kappa^2\omega_s^6 \end{pmatrix}}, \\ U_c(s) = \dfrac{F(s)s^2\omega_s(2s\xi + \kappa^2\omega_s)}{\begin{pmatrix} s^6(-1+\beta) + 2s^5(-1+(-1+\beta)\mu)\xi\omega_s + s^4(-1+\beta-\eta^2-\kappa^2-\kappa^2\mu+\beta\kappa^2\mu)\omega_s^2 \\ -2s^3\big(1+\eta^2(1+\mu)\big)\xi\omega_s^3 - s^2\left(\kappa^2+\eta^2\big(1+\kappa^2(1+\mu)\big)\right)\omega_s^4 - 2s\eta^2\xi\omega_s^5 - \eta^2\kappa^2\omega_s^6 \end{pmatrix}}, \end{cases} \tag{6}$$

$$\sigma_{U,S_0}^2 = \frac{\pi S_0}{2(-1+\beta+\eta^2)^2\kappa\mu\xi\omega_s^3}\left(\begin{array}{l}\beta^2\left(1+\kappa^2\mu(-1+\kappa^2\mu)\right)+(-1+\eta^2)^2\left(\begin{array}{l}1+\kappa^4(1+\mu)^2\\+\kappa^2(-2-\mu+4(1+\mu)\xi^2)\end{array}\right)\\+\beta\left(\begin{array}{l}-2\left(1+\kappa^2\left(-1+\mu(-1+\kappa^2(1+\mu)+2\xi^2)\right)\right)\\+\eta^2\left(2+\kappa^2\left(-2+\mu(-2+\kappa^2(3+2\mu)+8\xi^2)\right)\right)\end{array}\right)\end{array}\right) \tag{9}$$

whereas the structural acceleration response can be numerically calculated for a limited frequency band. To express the wind-induced excitation, the Davenport model is adopted for the stochastic response analysis (Davenport 1967)

$$S_f = \frac{2r^2}{3\Omega(1+r^2)^{\frac{4}{3}}}, r = \frac{600\Omega}{\pi v_{10}}, \tag{10}$$

where $v_{10} = 30\ \frac{m}{s}$ denotes the wind velocity at a height of 10 m, and Ω is the frequency component variable of wind-induced excitation.

3. Optimal design guides for ILDs

3.1 Performance indicators and overview

As multiperformance evaluators for wind-excited structures, the structural displacement response ratio γ_U and acceleration response ratio γ_A are defined in comparison with the uncontrolled original structures

$$\gamma_U = \frac{\sigma_U}{\sigma_{U,0}}, \quad \gamma_A = \frac{\sigma_A}{\sigma_{A,0}}. \tag{11}$$

where $\sigma_{U,0}$ and $\sigma_{A,0}$ denote the root-mean-square values of the displacement and acceleration responses of the original responses, respectively. To assess the required installation space, the isolation layer displacement ratio γ_{iso} is defined and normalized by $\sigma_{U,0}$ as

$$\gamma_{iso} = \frac{\sigma_{U_i}}{\sigma_{U,0}} \tag{12}$$

where σ_{U_i} denotes the root-mean-square value of the isolation layer displacement.

3.2 Parametric investigation

Considering the dual-tuning effect of the ILD, the wind-

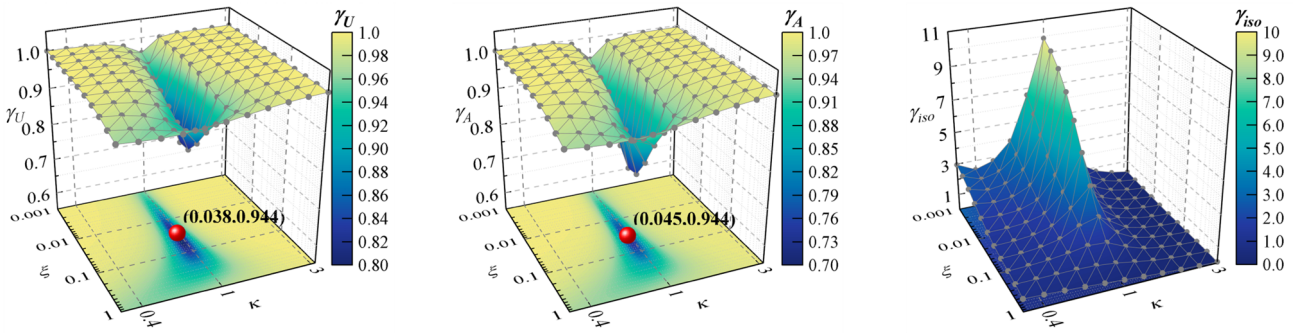

(a) (b) (c)

Fig. 5 Ratios of the responses of the wind-excited SDOF structure controlled by an isolated liquid damper (ILD) with liquid mass ratio $\mu = 0.01$, stiffness ratio $\kappa \in [0.3, 3.0]$, and damping ratio $\xi \in [0.001, 1.0]$: (a) displacement response ratio γ_U; (b) acceleration response ratio γ_A; and (c) isolation layer displacement response ratio γ_{iso}

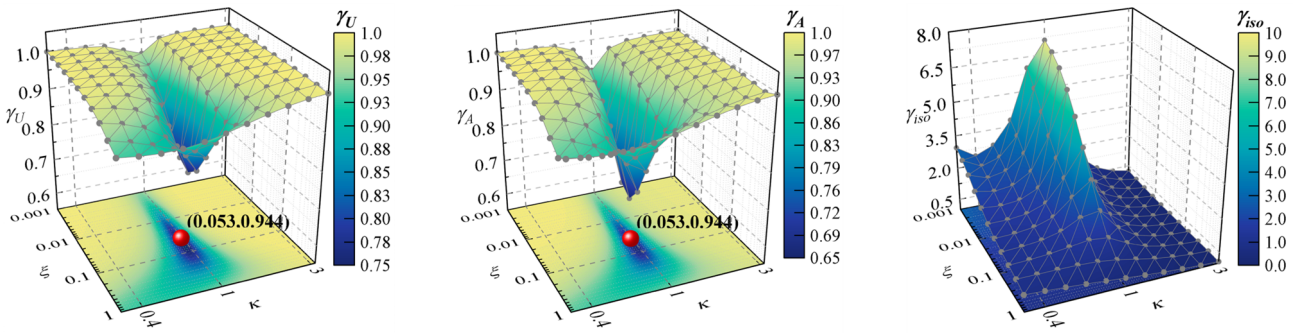

(a) (b) (c)

Fig. 6 Ratios of the responses of the wind-excited SDOF structure controlled by an isolated liquid damper (ILD) with liquid mass ratio $\mu = 0.02$, stiffness ratio $\kappa \in [0.3, 3.0]$, and damping ratio $\xi \in [0.001, 1.0]$: (a) displacement response ratio γ_U; (b) acceleration response ratio γ_A; and (c) isolation layer displacement response ratio γ_{iso}

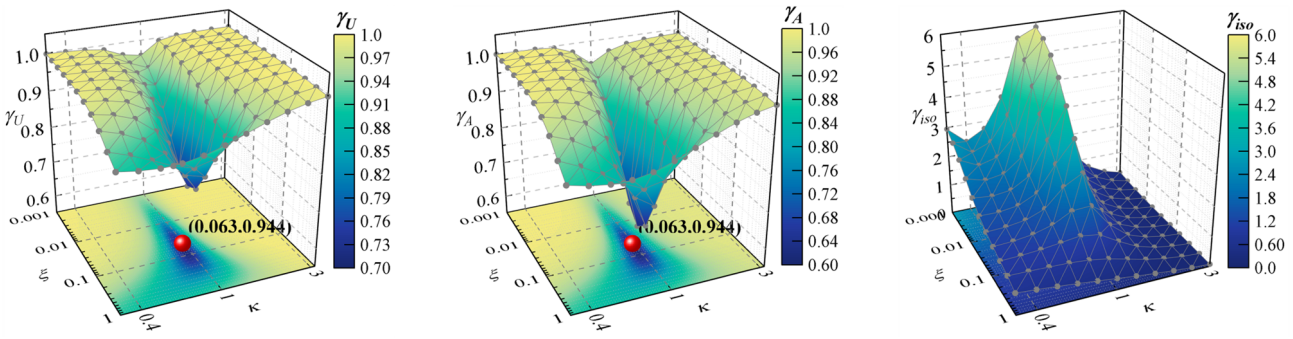

(a) (b) (c)

Fig. 7 Ratios of the responses of the wind-excited SDOF structure controlled by an isolated liquid damper (ILD) with liquid mass ratio $\mu = 0.03$, stiffness ratio $\kappa \in [0.3, 3.0]$, and damping ratio $\xi \in [0.001, 1.0]$: (a) displacement response ratio γ_U; (b) acceleration response ratio γ_A; and (c) isolation layer displacement response ratio γ_{iso}

induced vibration control effect can be determined by the installation characteristics, isolation parameters of the isolation layer, and liquid parameters. Subject to wind excitation with a narrow frequency bandwidth, the structural oscillation is dominated by the first mode in which the structural displacement is maximal at the top floor. To trigger the tuning motions of the ILD to the maximum extent, the ILD is proposed to be installed at the top of the structure. For this ILD, the undetermined design parameters include the isolation frequency ratio κ, isolation damping ratio ξ, liquid mass ratio μ, and $\frac{h}{L}$ (using these parameters, the liquid frequency ratio ω_c and convective mass ratio β can be determined). For constant liquid mass ratios $\mu =$ 0.01, 0.02, and 0.03 and tuned liquid element dimensions of $\frac{h}{L} = 0.60$, the contour plots of the structural displacement response ratio γ_U, acceleration response ratio γ_A, and isolation layer displacement ratio γ_{iso} are shown in Figa. 5 to 7. The liquid damping ratio $\xi_c = 0.005$ (Veletsos 1984, Fediw *et al.* 1995, Luo *et al.* 2016) is adopted as the typical value of water, which is widely used in building structures. For the primary structure, the structural mass is $m = 20$ ton, and the structural stiffness is $k = 790$ kN/m, corresponding to the undamped frequency of 1.0 Hz. The structural damping ratio is $\zeta =$ 0.015. The wind velocity v_{10} is assumed to be 35 $\frac{m}{s}$ as an example. For the ILD with variable isolation frequency ratio κ and isolation damping ratio ξ, the structural displacement and acceleration response ratios, γ_U and γ_A, exhibit valley-shaped curves. The bottom part demonstrates the greatest vibration control effects in terms of the structural displacement and acceleration responses. As the added liquid ratios μ increase from 0.01 to 0.03, the optimal locations corresponding to the lowest γ_U and γ_A are in agreement, implying dual-performance control for structural safety and serviceability. In particular, the ILD with a large liquid mass ratio μ must be optimized by using a larger isolation damping ratio ξ, even though the optimal isolation frequency ratio remains nearly constant, approaching unity. In terms of the installation space, the ILD with a large isolation damping ratio ξ is effective to ensure the energy dissipation and suppression of the displacement concentrated at the isolation layer. As κ approaches unity, the resonant motion results in a significant displacement response of the isolation layer, while the optimal isolation damping ratio ξ ensures intermediate or low values of γ_{iso}. When the isolation subsystem is designed using the optimal isolation parameters, the ILD exhibits a satisfactory vibration control capacity to alleviate the displacement and acceleration

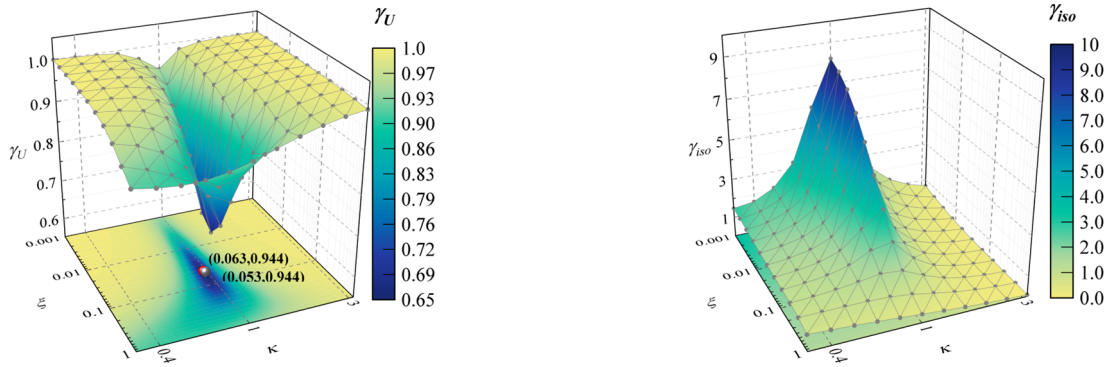

(a) γ_U (b) γ_{iso}

Fig. 8 Ratios of the responses of the SDOF structure controlled by an isolated liquid damper (ILD) with liquid mass ratio $\mu = 0.03$, stiffness ratio $\kappa \in [0.3, 3.0]$, and damping ratio $\xi \in [0.001, 1.0]$ subject to white noise

responses of the wind-excited structure, which can enhance the wind-induced safety and occupant comfort. Moreover, the installation space required by the insert of an isolation subsystem can be optimally decreased by the damping effect, which can promote the applicability of the device in practical building structures To utilize the closed-form response expression of the ILD-equipped structure excited by white noise, the difference in the optimal isolation frequency ratio κ and damping ratio ξ between the white noise and wind loads are investigated, as indicated in Fig. 8.

Considering the liquid mass ratio $\mu = 0.03$ as an example, to maximize the displacement response mitigation effect, the optimal isolation frequency ratios are maintained nearly constant under the two types of excitations. However, the isolation damping ratio optimized in the white noise condition is smaller than that in the wind load condition, implying that a large damping ratio ξ is required to satisfy the vibration control demand yielded from the excitation with a narrow frequency bandwidth. Comparing the installation space required in the two types of excitations, the isolation layer displacement responses shown in Fig. 8(b) and Fig. 7(c) demonstrate similar vibration patterns, although a larger γ_{iso} can be noted for the ILD-equipped structure subject to white noise. In this situation, the optimal isolation parameters derived under the assumption of white noise can help establish a wind-excited structure with a satisfactory dual-performance control effect and decreased installation space.

3.3 Analytical design formulae

Considering the results associated with white noise and wind-induced excitations, analytical design formulae are derived to facilitate the preliminary design of ILDs for wind-induced vibration control. To determine the closed-form isolation frequency ratio κ and damping ratio ξ, the optimization problem can be defined by setting the partial derivatives of the analytical displacement response γ_U^2 specified in Eq. (9) with respect to κ and ξ as zero

$$\frac{\partial \gamma_U^2}{\partial \kappa} = 0, \quad \frac{\partial \gamma_U^2}{\partial \xi} = 0. \tag{13}$$

Substituting Eqs. (9) and (11) into Eq. (13), the optimal values of κ and ξ can be theoretically derived as

$$\begin{cases} \kappa_{opt} = \dfrac{\sqrt{(-1+\beta+\eta^2)\left(-2+(-1+\beta)\mu+\eta^2(2+\mu)\right)}}{\sqrt{2}\sqrt{\eta^4(1+\mu)^2+(-1+(-1+\beta)\mu)^2+\eta^2\left(-2+\mu(-4+3\beta+2(-1+\beta)\mu)\right)}} \\ \xi_{opt} = \dfrac{1}{4\kappa_{opt}}\sqrt{\dfrac{\mu(4(1-\beta+2(-1+\beta)\eta^2+\eta^4)+3(-1+\beta+\eta^2)^2\mu)}{\left[\left(1+\mu-\beta\mu+\eta^4(1+\mu)+2\eta^2(-1+(-1+\beta)\mu)\right)\cdot \left(\eta^4(1+\mu)^2+(-1+(-1+\beta)\mu)^2+\eta^2\left(-2+\mu(-4+3\beta+2(-1+\beta)\mu)\right)\right)\right]}}\,|-1+\beta+\eta^2| \end{cases} \tag{14}$$

The derived analytical design formulae are easy-to-use and can be simply applied to estimate the optimal isolation frequency and damping ratios of the ILD, thereby enhancing the serviceability of wind-excited structures. More accurate optimization results can be numerically obtained through optimization tools by solving the optimization problem specified in Section 3.5.

3.4 Robustness analysis

The installation of an additional isolation layer in the ILD facilitates highly efficient energy storage and absorption through the inertia of nearly the entire liquid mass. In this situation, the ILD is expected to be superior to a TLD with the same tuned liquid element and can be used to substitute conventional tuned mass dampers (TMDs). To demonstrate this advantage, the structural displacement responses in the frequency domain for the original structure and structures with the TMD, TLD, and ILD subjected to wind excitations are plotted in Fig. 9(a). The tuned-type dampers are designed with the same additional mass ratio $\mu = 0.02$ and $h/L = 0.6$. Two TLDs are compared, with the nonoptimal TLD designed to have the tuned liquid element described in Section 3.2, and the other TLD optimized similar to the TMD (Tait 2008). This TLD can be physically realized by changing the shape of the liquid tank and adding several liquid screens. The isolation subsystems of the ILD and TMD are optimized using Eq. (14) and the fixed-point method. Compared with those of the original structure, the resonant responses of the ILD/TLD-equipped structure are significantly suppressed due to the tuning mechanism of the liquid-based damper. In terms of the control performance in the frequency domain, the frequency band for effective vibration control is defined as the excitation frequency when the displacement response of the controlled structure is smaller than that of the original structure. Benefiting from the outside isolation subsystem in the ILD, especially easy-to-implement damping effects, the structural displacement peaks can be suppressed more remarkably in the frequency domain with a larger bandwidth. For the ILD and TMD with the same mass ratios, similar vibration mitigation effects can be observed, although the ILD exhibits a larger frequency bandwidth owing to the multimode vibration of the liquid. The comparison of the isolation subsystem deformations of the ILD and TMD, shown in Fig. 9(b), demonstrates that the isolation subsystem in the ILD can oscillate with lower amplitudes in the larger frequency bandwidth.

Considering practical application scenarios in which the tuned liquid element is characterized by different $\frac{h}{L}$ values owing to the daily usage requirement, the effectiveness of the TLD and ILD for vibration control is evaluated by

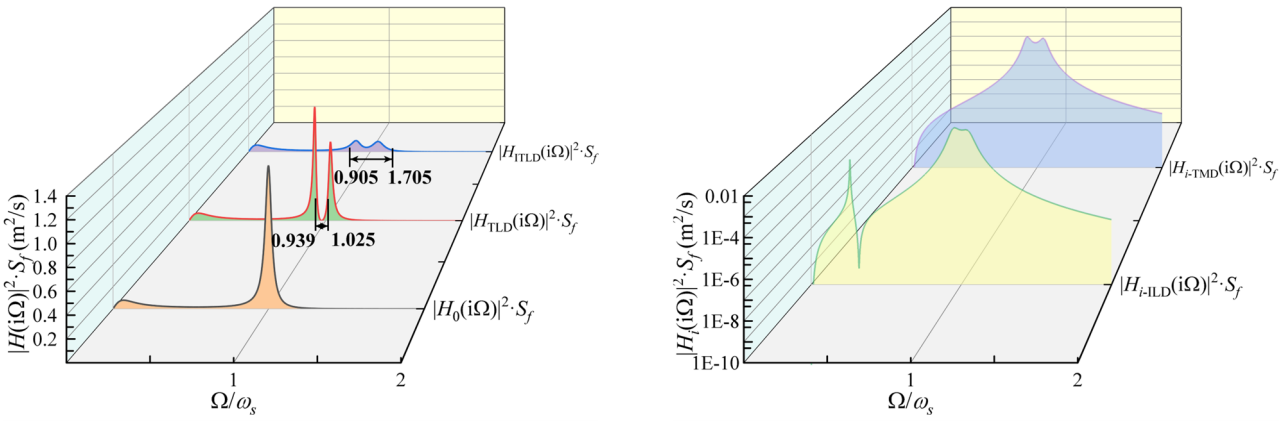

(a) (b)

Fig. 9 Frequency response of (a) the original SDOF structure, SDOF-TLD, SDOF-ILD, and SDOF-TMD; and (b) the isolation deformation subjected to wind excitation (wind velocity $v_{10} = 35\ \frac{m}{s}$)

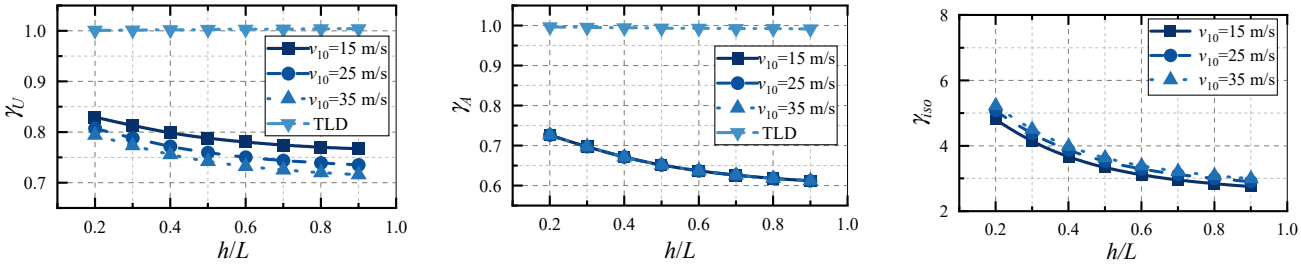

(a) γ_U (b) γ_A (c) γ_{iso}

Fig. 10 Dynamic response ratios of the SDOF structure controlled by an isolated liquid damper (ILD) with liquid mass ratio $\mu = 0.02$, optimized stiffness ratio κ, optimized damping ratio ξ, and variable liquid height ratios $\frac{h}{L}$ subject to wind excitation

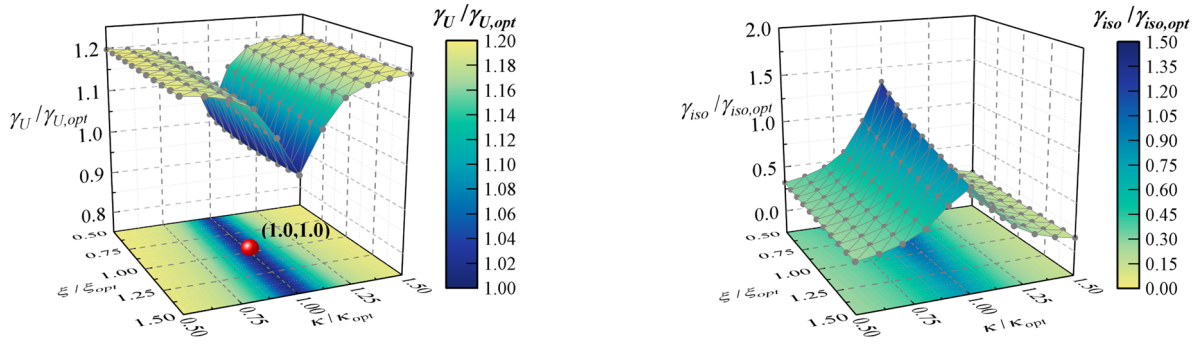

(a) $\gamma_U/\gamma_{U,opt}$ (b) $\gamma_{iso}/\gamma_{iso,opt}$

Fig. 11 Response ratios of the SDOF structure controlled by an ILD with $\mu = 0.02$, $\kappa \in [0.50, 1.50]\kappa_{opt}$, and $\xi \in [0.50, 1.50]\xi_{opt}$ subjected to wind excitation

considering γ_U, γ_A, and γ_{iso} against $\frac{h}{L}$ varying from 0.20 to 0.70. For a liquid mass ratio $\mu = 0.02$, considered as an example, the vibration control performances γ_U, γ_A, and γ_{iso} for ILD- and TLD-equipped structures subject to wind loads with different velocities are shown in Fig. 10. To ensure a fair comparison, the ILD is designed using Eq. (14), whereas the TLD is designed to have the same tuned liquid element as the ILD (corresponding to the non-optimized TLD). The comparative results of the ILD and TLD indicate that the ILD exhibits a superior wind-induced vibration control effect for the multilevel wind loads.

Notably, the use of an existing water tank that is not designed for vibration control in the TLD can adversely influence wind-induced vibration control. In contrast, when the designed isolation subsystem is applied, the ILD can be easily implemented to significantly mitigate the wind-

induced structural responses, and the system performance is robust against types of water tanks with variable liquid depths.

As an objective drawback of the dynamic vibration absorber, the control performance is sensitive to changes in the stiffness and damping components owing to possible manufacturing errors. To quantify the robustness of ILD for wind-induced vibration control under the condition of nonoptimal design parameters, a parametric analysis is performed for an ILD with various isolation frequency ratios κ and damping ratios ξ. Assuming constant key parameters of the tuned liquid element, the disturbances of ξ and κ are set to be in the range of 50% variation of ξ_{opt} and κ_{opt} specified using from Eq. (14).

In terms of the structural displacement response in Fig. 11, γ_U changes in a relatively small variation range $[1.0-1.2]$. The nonoptimal control performances corresponding to $\gamma_U > 1.0$ may be accompanied by a lower requirement of installation space evaluated by γ_{iso}. Under this condition, the nonoptimal isolation parameters do not notably degrade the wind-induced vibration control effect of the ILD, which is thus robust and practical to enhance the wind-resistance performance of buildings.

3.5 Serviceability-oriented design procedure

The abovementioned analysis results indicate that the ILD serves as a robust and economical tool to control the wind-induced vibration of structures, as the liquid inertia of an existing liquid tank can be exploited without affecting its original functionality. Utilizing the dual-performance control advantage of ILDs, a serviceability-oriented design method is established to simultaneously decrease the structural displacement and acceleration responses, shown in Fig. 12. Considering the serviceability-based control demand, i.e., the target structural response ratio of acceleration $\gamma_{A,T}$, the structure displacement response ratio can be minimized as

$$\begin{cases}\text{minimize} & \gamma_U(\mu,\kappa,\xi,\xi_c,\eta)\\ \text{subject to} & \gamma_A(\mu,\kappa,\xi,\xi_c,\eta)\le\gamma_{A,T}\end{cases}. \tag{15}$$

To manufacture an ILD, two implementations can be considered, that is, the TLD with and without a pre-existing tuned liquid element. To enhance the existing liquid tank, the optimal design method in Eq. (15) can be adopted to determine the key parameters of the isolation subsystem, thereby maximizing the wind-induced vibration mitigation

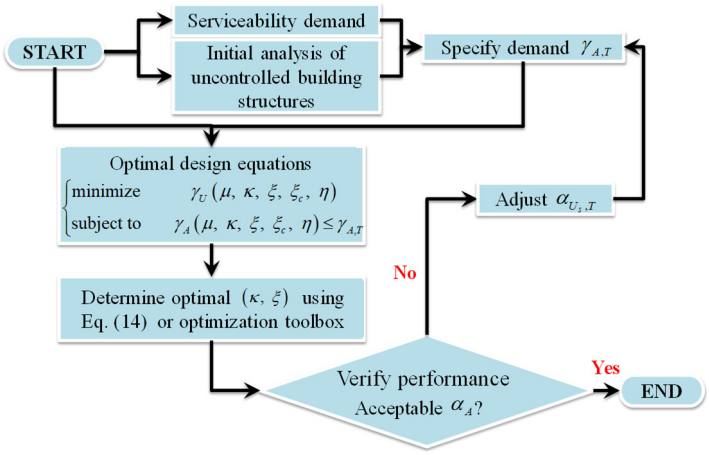

Fig. 12 Design procedure of the serviceability-oriented design for an ILD

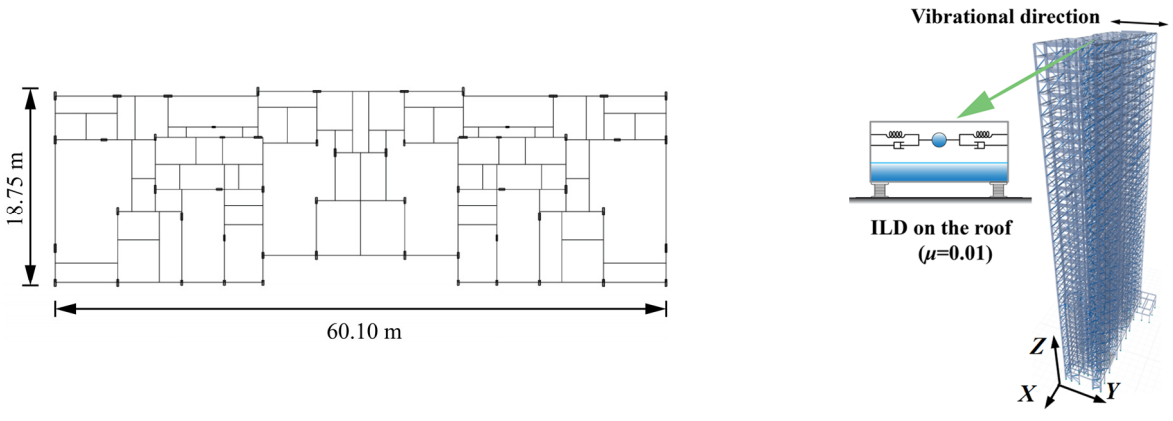

(a) Plan view (b) Perspective view

Fig. 13 Model of the considered high-rise building equipped with an ILD (μ denotes the liquid mass ratio of the ILD)

effect of the liquid tank. The optimal relationship can be numerically obtained from the 'fmincon' toolbox in MATLAB or preliminarily from the analytical design formulae presented as Eq. (15). Subsequently, the required liquid mass ratio can be calculated under the constrained condition of serviceability demand $\gamma_{A,T}$. The proposed design procedure is illustrated in the following figure.

4. Application of ILD in a wind-excited tall building

4.1 Information regarding the illustrative cases

As shown in Fig. 13, a steel high-rise building is employed to illustrate the effectiveness and applicability of ILDs in practical engineering. The selected structure consists of 44 stories and 145.95 m high, of which the perimeter dimension is 60.10 m × 18.75 m, shown in Fig. 13. Simulated by ETABS software (ETABS 2021), the material of the structural frames and braces is steel. Rigid diaphragms are employed for the floors, limiting the in-plane translation and out-of-plane rotation of nodes on each floor. Translation DOFs of nodes on the same rigid diaphragm are coupled, with the system matrices automatically assembled in ETABS. Utilizing the lumped mass matrix, the high-rise building model is constructed with 8,062 nodes. The numerical simulation is conducted in the Y-Z plane, assigning 3 DOFs to each node. Consequently, the system matrices have dimensions of 24,186 × 24,186. Additional details regarding the building can be found in a technical report (Shanghai Research Institute of Materials 2018). To perform the wind vibration analysis, the Rayleigh damping is taken as 0.02 for steel structures. Translations in Y-Z plane and rotations about X axis are considered and 150 modes are included in the analysis. The oscillating periods of the first two modes of the considered building are obtained as 6.207 and 1.793 s, respectively.

The wind tunnel test (Shanghai Research Institute of Materials 2018) was performed at the Wind Tunnel Laboratory of the State Key Laboratory for Disaster Reduction in Civil Engineering, Tongji University. The wind load time history comprises time series of aerodynamic force for measurement locations on the high-rise building, obtained from a wind tunnel test on a rigid model. A basic wind pressure of 0.4 kPa, corresponding to 10-year wind, is adopted herein. The current study focuses on an along-wind response control for the buildings.

4.2 Optimization of ILD

To implement an ILD on the roof, at which the largest vibration amplitudes occur under wind excitation, the undetermined design parameters of the ILD can be optimized to mitigate the wind-induced responses of the high-rise structure. The target vibration control performance is determined as $\gamma_{A,T} = 0.70$. By substituting $\gamma_{A,T} = 0.70$

Table 2 Optimal parameters of the designed ILD

Control device	Isolation layer		Convective mass		
	μ	m_l	β	m_c	h/L
ILD (44th floor)	0.01	410 ton	0.32	194 ton	0.8
	k_i	c_i	k_c		c_c
	419 kN/m	41.8 kN · s/m	2383 kN/m		6.8 kN · s/m

Table 3 Dynamic responses of the original building and building with an ILD

Response	Acceleration responses (mm/s^2)			Displacements responses (mm)		
	ST0	ST1	ST2	ST0	ST1	ST2
Peak	118.5	86.1(-27.3%)	98.0 (-17.3%)	140.8	107.2 (-23.8%)	119.8 (-14.9%)
Root-mean-square	35.9	24.9 (-30.8%)	27.1 (-24.5%)	41.0	31.1 (-23.0%)	35.2 (-14.0%)

*Note: ST0-original building, ST1-building-ILD, and ST2-building-TLD

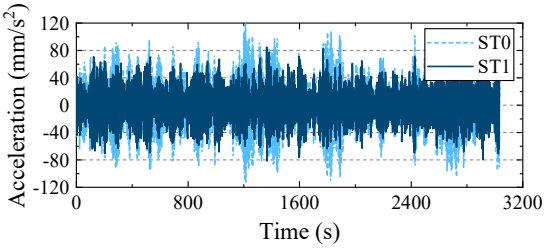

(a) Roof acceleration history

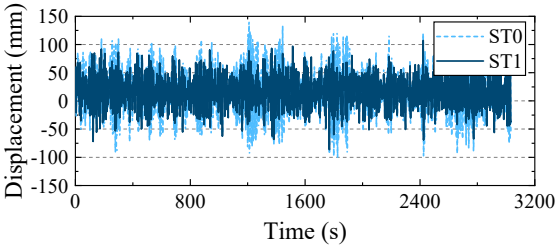

(b) Roof displacement history

Fig. 14 Responses of the original high-rise building and building with an ILD under the input wind excitation

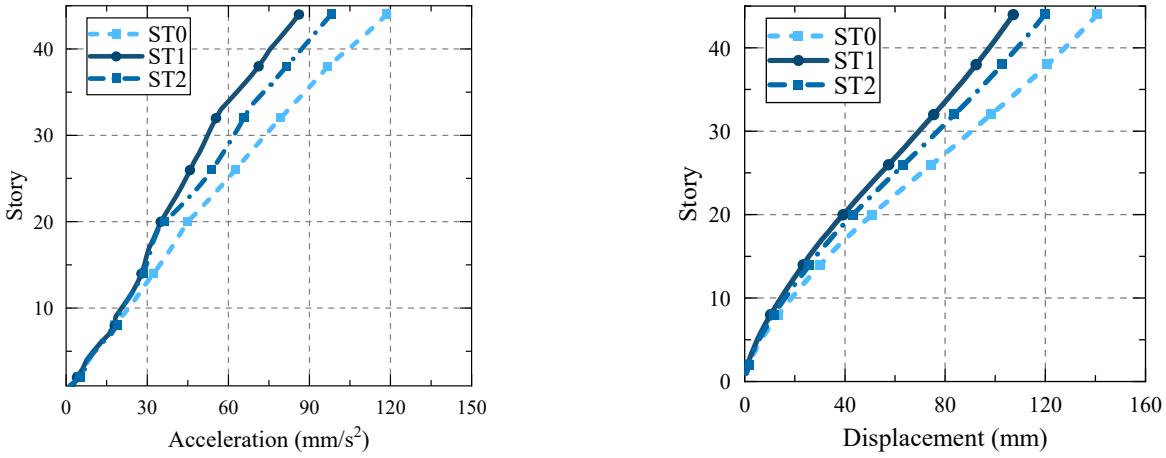

(a) Root-mean-square acceleration

(b) Maximum displacement

Fig. 15 Responses on each story of the original high-rise building and building with an ILD subjected to wind excitation

into Eq. (15), the optimal parameters of the ILD can be initially designed by Eq. (14) and numerically calculated from the 'fmincon' (Byrd *et al*. 2000) toolbox. Notably, the design outcomes from both methods closely align with each other, leading to the presentation of the direct design results Eq. (14) is presented in Table 2. Specifically, the tuned liquid tank is characterized by the length 16 m, width 5.7 m, and height 4.5 m.

4.3 Performance assessment of the ILD-equipped building by wind loads

Addressing the wind-induced response mitigation effect of the ILD, the transient analysis is executed for typical wind excitation, the historical record of which is obtained through a wind tunnel experiment. The roof acceleration and displacement responses for the original high-rise building (ST0) and ILD-equipped building (ST1) are summarized in Table 3 and plotted in Fig. 14. Due to the high performance of the ILD relative to the wind-induced vibration control, the structural displacement and acceleration are significantly suppressed in terms of the peak and root-mean-square values. Specifically, the reductions in the peak and root-mean-square values are -27.3% and -30.8% for the roof acceleration, respectively, whereas those for the roof displacement are -23.8% and -23.0%, respectively.

To demonstrate the advantages of the ILD over the conventional TLD, the dynamic responses of ST0 and ST1 for each story under wind excitation are shown in Fig. 15, where the TLD (ST2) is designed to have the same liquid mass and optimized based on the TMD. The optimized TLD can be physically realized by changing the shape of the liquid tank and adding liquid screens. Consistent with the parametric analysis and optimal design target specified in Sections 3.2 and 3.5, the acceleration and displacement responses of the entire high-rise building are effectively decreased by the ILD, and the TLD demonstrates a low-level reduction capacity. Owing to the dual-isolating capacity of the ILD, the structural serviceability and safety can be simultaneously enhanced, which cannot be realized using an existing liquid tank without optimized damping technology.

5. Conclusions

This study proposes a serviceability-oriented optimal design method for ILDs and derives analytical design formulae to enable the practical design of wind-excited structures. Utilizing the damping effect provided from the outside of liquid tanks, no liquid screens are required in ILDs to improve the damping performance of liquid, which can be treated as a more realistic and practical solution for wind-induced vibration control. The key conclusions of this study can be summarized as follows:

- The high-level serviceability demand can be effectively satisfied by the ILD based on the proposed optimal design framework. Specifically, the optimal mitigation condition can be realized when the entire liquid mass is tuned to the dominant frequency of the targeted structure.
- The proposed serviceability-oriented design method can ensure the comfort demand of the primary structure target with optimally suppressed displacement responses. Specifically, the analytical design formulae can be preliminarily adopted to define the optimal design relationship between the parameters of the liquid mass and isolation subsystem.
- Owing to the added isolation subsystem, top-placed ILDs can provide higher effectiveness and larger frequency bandwidth to enable the robust mitigation of multiple wind-induced responses of high-rise buildings. Compared with the conventional TLD based on the same design parameters, the ILDs exhibit enhanced vibration control effects under multi-intensity wind conditions.
- The ILD can realize robust wind-induced vibration control, and its control capacity is not sensitive to the change in liquid parameters, even under non-

optimal conditions of the isolation subsystem. Pertinent wind tunnel tests must be performed to verify the effectiveness of the ILDs for wind-excited structures.

Acknowledgments

This study was supported by the National Natural Science Foundation of China (Grant No. 52308525), 2024 Open Project of Failure Mechanics and Engineering Disaster Prevention, Key Lab of Sichuan Province (FMEDP202402), Chunhui Plan of Cooperative Research Project of Ministry of Education (Grant No. HZKY20220228), Science and Technology Foundation of Gansu Province (Grant No. 23JRRA801), and Red Willow Excellent Young Talent Support Plan of Lanzhou University of Technology.

References

Banerji, P., Murudi, M., Shah, A.H. and Popplewell, N. (2000), "Tuned liquid dampers for controlling earthquake response of structures", *Earthq. Eng. Struct. Dyn.*, **29**(5), 587-602. https://doi.org/10.1002/(SICI)1096-9845(200005)29:5<587::AID-EQE926>3.0.CO;2-I

Bauer, H.F. (1984), "Oscillations of immiscible liquids in a rectangular container - A new damper for excited structures", *J. Sound Vib.*, **93**(1), 117-133. https://doi.org/10.1016/0022-460x(84)90354-7

Byrd, R.H., Gilbert, J.C. and Nocedal, J. (2000), "A trust region method based on interior point techniques for nonlinear programming", *Mathe. Programm.*, **89**(1), 149-185. https://doi.org/10.1007/PL00011391

Chang, C.C. and Qu, W.L. (1998), "Unified dynamic absorber design formulas for wind-induced vibration control of tall buildings", *Struct. Des. Tall Build.*, **7**(2), 147-166. https://doi.org/10.1002/(SICI)1099-1794(199806)7:2<147::AID-TAL107>3.0.CO;2-3

Chen, Q., Zhao, Z., Xia, Y., Pan, C., Luo, H. and Zhang, R. (2019), "Comfort based floor design employing tuned inerter mass system", *J. Sound Vib.*, **458**, 143-157. https://doi.org/10.1016/j.jsv.2019.06.019

Crandall, S.H. and Mark, W.D. (1963), Random Vibration in Mechanical System.

Davenport, A.G. (1967), "Gust loading factors", *J. Struct. Div.*, **93**(3), 11-34. https://doi.org/10.1061/JSDEAG.0001692

Elias, S. and Matsagar, V. (2017), "Research developments in vibration control of structures using passive tuned mass dampers", *Annual Rev. Control*, **44**, 129-156. https://doi.org/10.1016/j.arcontrol.2017.09.015

Elias, S. and Matsagar, V. (2018), "Wind response control of tall buildings with a tuned mass damper", *J. Build. Eng.*, **15**, 51-60. https://doi.org/10.1016/j.jobe.2017.11.005

ETABS (2021), Building analysis and design; from https://www.csiamerica.com/products/etabs

Fediw, A.A., Isyumov, N. and Vickery, B.J. (1995), "Performance of a tuned sloshing water damper", *J. Wind Eng. Industr. Aerodyn.*, **57**(2), 237-247. https://doi.org/10.1016/0167-6105(94)00107-O

Furtmüller, T., Di Matteo, A., Adam, C. and Pirrotta, A. (2019), "Base-isolated structure equipped with tuned liquid column damper: An experimental study", *Mech. Syst. Signal Process.*, **116**, 816-831. https://doi.org/10.1016/j.ymssp.2018.06.048

Gaur, S., Elias, S., Höbbel, T., Matsagar, V.A. and Thiele, K. (2020), "Tuned mass dampers in wind response control of wind turbine with soil-structure interaction", *Soil Dyn. Earthq. Eng.*, **132**, 106071. https://doi.org/10.1016/j.soildyn.2020.106071

Hu, X., Zhao, Z., Yang, K., Liao, W. and Chen, Q. (2023a), "Novel triple friction pendulum-tuned liquid damper for the wind-induced vibration control of airport control towers", *Thin-Wall. Struct.*, **182**, 110337. https://doi.org/10.1016/j.tws.2022.110337

Hu, X., Zhao, Z., Zhang, R., Yang, K., Chen, Q. and Weng, D. (2023b), "Seismic resilient design and negative stiffness-assisted nonlinear isolation system for adjacent non-coaxial buildings linked by corridors", *Soil Dyn. Earthq. Eng.*, **175**, 108227. https://doi.org/10.1016/j.soildyn.2023.108227

Huang, M.F., Chan, C.M. and Lou, W.J. (2012), "Optimal performance-based design of wind sensitive tall buildings considering uncertainties", *Comput. Struct.*, **98-99**, 7-16. https://doi.org/10.1016/j.compstruc.2012.01.012

Islam, N.U. and Jangid, R.S. (2022), "Optimum parameters of tuned inerter damper for damped structures", *J. Sound Vib.*, **537**, 117218. https://doi.org/10.1016/j.jsv.2022.117218

Jangid, R.S. and Banerji, P. (1998), "Effects of isolation damping on stochastic response of structures with nonlinear base isolators", *Earthq. Spectra*, **14**(1), 95-114. https://doi.org/10.1193/1.1585990

Jangid, R.S. and Datta, T.K. (1995), "Seismic behaviour of base-isolated buildings: A state-of-the art review", *Proceedings of the Institution of Civil Engineers-Structures and Buildings*, **110**(2), 186-203. https://doi.org/10.1680/istbu.1995.27599

Kareem, A. (2020), "Emerging frontiers in wind engineering: Computing, stochastics, machine learning and beyond", *J. Wind Eng. Industr. Aerodyn.*, **206**, 104320. https://doi.org/10.1016/j.jweia.2020.104320

Lee, C.S., Love, J.S., Haskett, T.C. and Robinson, J.K. (2021), "Concept design of a parallel-type tuned mass damper-tuned sloshing damper system for building motion control in wind", *Int. J. High-Rise Build.*, **10**(2), 93-97. https://doi.org/10.21022/IJHRB.2021.10.2.93

Love, J.S. and Tait, M.J. (2010), "Nonlinear simulation of a tuned liquid damper with damping screens using a modal expansion technique", *J. Fluids Struct.*, **26**(7), 1058-1077. https://doi.org/10.1016/j.jfluidstructs.2010.07.004

Love, J.S., McNamara, K.P., Tait, M.J. and Haskett, T.C. (2019), "Series-type pendulum tuned mass damper-tuned sloshing damper", *J. Vib. Acoust.*, **142**(1). https://doi.org/10.1115/1.4044866

Lu, Z., Wang, D., Masri, S.F. and Lu, X. (2016), "An experimental study of vibration control of wind-excited high-rise buildings using particle tuned mass dampers", *Smart Struct. Syst., Int. J.*, **18**(1), 93-115. https://doi.org/10.12989/sss.2016.18.1.093

Lu, L.Y., Lin, G.L., Chen, Y.S. and Hsiao, K.A. (2020a), "Vertical equipment isolation using piezoelectric inertial-type isolation system", *Smart Struct. Syst., Int. J.*, **26**(2), 195-211. https://doi.org/10.12989/sss.2020.26.2.195

Lu, Z.Q., Shao, D., Fang, Z.W., Ding, H. and Chen, L.Q. (2020b), "Integrated vibration isolation and energy harvesting via a bistable piezo-composite plate", *J. Vib. Control*, **26**(9-10), 779-789. https://doi.org/10.1177/1077546319889815

Luo, H., Zhang, R. and Weng, D. (2016), "Mitigation of liquid sloshing in storage tanks by using a hybrid control method", *Soil Dyn. Earthq. Eng.*, **90**, 183-195. https://doi.org/10.1016/j.soildyn.2016.08.037

Marian, L. and Giaralis, A. (2017), "The tuned mass-damper-inerter for harmonic vibrations suppression, attached mass reduction, and energy harvesting", *Smart Struct. Syst., Int. J.*, **19**(6), 665-678. https://doi.org/10.12989/sss.2017.19.6.665

Mensah, A.F. and Duenas-Osorio, L. (2014), "Improved reliability of wind turbine towers with tuned liquid column dampers (TLCDs)", *Struct. Safety*, **47**, 78-86.

https://doi.org/10.1016/j.strusafe.2013.08.004
Niu, H., Chen, Z., Hua, X. and Zhang, W. (2018), "Mitigation of wind-induced vibrations of bridge hangers using tuned mass dampers with eddy current damping", *Smart Struct. Syst., Int. J.*, **22**(6), 727-741. https://doi.org/10.12989/sss.2018.22.6.727
Pandey, D.K., Sharma, M.K. and Mishra, S.K. (2019), "A compliant tuned liquid damper for controlling seismic vibration of short period structures", *Mech. Syst. Signal Process.*, **132**, 405-428. https://doi.org/10.1016/j.ymssp.2019.07.002
Roy, A., Zhang, Z., Ghosh, A. and Basu, B. (2019), "On the nonlinear performance of a tuned sloshing damper under small amplitude excitation", *J. Vib. Control*, **25**(21-22), 2695-2705. https://doi.org/10.1177/1077546319867232
Ruiz, R.O., Lopez-Garcia, D. and Taflanidis, A.A. (2016), "Modeling and experimental validation of a new type of tuned liquid damper", *Acta Mechanica*, **227**(11), 3275-3294. https://doi.org/10.1007/s00707-015-1536-7
Sato, T. (1987), "Tuned sloshing damper", *J. Wind Eng.*, **32**, 67-68.
Shanghai Research Institute of Materials (2018), Design Report on Energy Dissipation and Seismic Reduction of Building B of Heng Yu Financial Center; Shanghai Research Institute of Materials, Shanghai, China.
Soong, T.T. and Spencer Jr., B.F. (2002), "Supplemental energy dissipation: state-of-the-art and state-of-the-practice", *Eng. Struct.*, **24**(3), 243-259. https://doi.org/10.1016/S0141-0296(01)00092-X
Sun, L.M. and Fujino, Y. (1994), "A semi-analytical model for tuned liquid damper (TLD) with wave breaking", *J. Fluids Struct.*, **8**(5), 471-488. https://doi.org/10.1006/jfls.1994.1023
Suthar, S.J. and Jangid, R.S. (2021a), "Design of tuned liquid sloshing dampers using nonlinear constraint optimization for across-wind response control of benchmark tall building", *Structures*. **33**, 2675-2688. https://doi.org/10.1016/j.istruc.2021.05.059
Suthar, S.J. and Jangid, R.S. (2021b), "Multiple tuned liquid sloshing dampers for across-wind response control of benchmark tall building", *Innov. Infrastr. Solut.*, **7**(1), 55. https://doi.org/10.1007/s41062-021-00650-6
Suthar, S.J. and Jangid, R.S. (2022), "Optimal design of tuned liquid column damper for wind-induced response control of benchmark tall building", *J. Vib. Eng. Technol.*, **10**(8), 2935-2945. https://doi.org/10.1007/s42417-022-00528-6
Tait, M.J. (2008), "Modelling and preliminary design of a structure-TLD system", *Eng. Struct.*, **30**(10), 2644-2655. https://doi.org/10.1016/j.engstruct.2008.02.017
Tait, M.J., Isyumov, N. and El Damatty, A.A. (2008), "Performance of tuned liquid dampers", *J. Eng. Mech.*, **134**(5), 417-427. https://doi.org/10.1061/(ASCE)0733-9399(2008)134:5(417)
Tamura, Y., Fujii, K., Ohtsuki, T., Wakahara, T. and Kohsaka, R. (1995), "Effectiveness of tuned liquid dampers under wind excitation", *Eng. Struct.*, **17**(9), 609-621. https://doi.org/10.1016/0141-0296(95)00031-2
Tanveer, M., Usman, M., Khan, I.U., Farooq, S.H. and Hanif, A. (2020), "Material optimization of tuned liquid column ball damper (TLCBD) for the vibration control of multi-storey structure using various liquid and ball densities", *J. Build. Eng.*, **32**, 101742. https://doi.org/10.1016/j.jobe.2020.101742
Veletsos, A.S. (1984), "Seismic response and design of liquid storage tanks", In: *Guidelines for the seismic design of oil and gas pipeline systems*, pp. 255-370.
Wang, Q., Qiao, H., De Domenico, D., Zhu, Z. and Tang, Y. (2021), "Seismic performance of optimal Multi-Tuned Liquid Column Damper-Inerter (MTLCDI) applied to adjacent high-rise buildings", *Soil Dyn. Earthq. Eng.*, **143**, 106653. https://doi.org/10.1016/j.soildyn.2021.106653
Yalla, S.K. and Kareem, A. (2000), "Optimum absorber parameters for tuned liquid column dampers", *J. Struct. Eng.*, **126**(8), 906-915. https://doi.org/10.1061/(ASCE)0733-9445(2000)126:8(906)
Yalla, S.K., Kareem, A. and Kantor, J.C. (2001), "Semi-active tuned liquid column dampers for vibration control of structures", *Eng. Struct.*, **23**(11), 1469-1479. https://doi.org/10.1016/S0141-0296(01)00047-5
Yucel, M., Bekdaş, G., Nigdeli, S.M. and Sevgen, S. (2019), "Estimation of optimum tuned mass damper parameters via machine learning", *J. Build. Eng.*, **26**, 100847. https://doi.org/10.1016/j.jobe.2019.100847
Zhao, Z., Zhang, R., Jiang, Y. and Pan, C. (2019), "A tuned liquid inerter system for vibration control", *Int. J. Mech. Sci.*, **164**, 105171. https://doi.org/10.1016/j.ijmecsci.2019.105171
Zhao, Z., Chen, Q., Zhang, R., Pan, C. and Jiang, Y. (2020), "Energy dissipation mechanism of inerter systems", *Int. J. Mech. Sci.*, **184**, 105845. https://doi.org/10.1016/j.ijmecsci.2020.105845
Zhao, Z., Zhang, R., Wierschem, N.E., Jiang, Y. and Pan, C. (2021), "Displacement mitigation–oriented design and mechanism for inerter-based isolation system", *J. Vib. Control*, **27**(17-18), 1991-2003. https://doi.org/10.1177/1077546320951662
Zhao, Z., Wang, Y., Hu, X. and Weng, D. (2022), "Seismic performance upgrading of containment structures using a negative-stiffness amplification system", *Eng. Struct.*, **262**, 114394. https://doi.org/10.1016/j.engstruct.2022.114394
Zhao, Z., Chen, Q., Hu, X. and Zhang, R. (2023), "Enhanced energy dissipation benefit of negative stiffness amplifying dampers", *Int. J. Mech. Sci.*, **240**, 107934. https://doi.org/10.1016/j.ijmecsci.2022.107934